ARL-TR-9816 ● Oct 2023

Improving Polytype Identification of Silicon Carbide Using Dictionary Indexing

by Jonathan Ligda

NOTICES

Disclaimers

The findings in this report are not to be construed as an official Department of the Army position unless so designated by other authorized documents.

Citation of manufacturer's or trade names does not constitute an official endorsement or approval of the use thereof.

Destroy this report when it is no longer needed. Do not return it to the originator.

ARL-TR-9816 ● OCT 2023

Improving Polytype Identification of Silicon Carbide Using Dictionary Indexing

Jonathan Ligda
DEVCOM Army Research Laboratory

REPORT DOCUMENTATION PAGE

1. REPORT DATE	2. REPORT TYPE	3. DATES COVERED	
		START DATE	END DATE
October 2023	Technical Report	3 October 2022	20 September 2023

4. TITLE AND SUBTITLE
Improving Polytype Identification of Silicon Carbide Using Dictionary Indexing

5a. CONTRACT NUMBER	5b. GRANT NUMBER	5c. PROGRAM ELEMENT NUMBER
5d. PROJECT NUMBER	**5e. TASK NUMBER**	**5f. WORK UNIT NUMBER**

6. AUTHOR(S)
Jonathan Ligda

7. PERFORMING ORGANIZATION NAME(S) AND ADDRESS(ES)	8. PERFORMING ORGANIZATION REPORT NUMBER
DEVCOM Army Research Laboratory ATTN: FCDD-RLA-MB Aberdeen Proving Ground, MD 21005	ARL-TR-9816

9. SPONSORING/MONITORING AGENCY NAME(S) AND ADDRESS(ES)	10. SPONSOR/MONITOR'S ACRONYM(S)	11. SPONSOR/MONITOR'S REPORT NUMBER(S)

12. DISTRIBUTION/AVAILABILITY STATEMENT
DISTRIBUTION STATEMENT A. Approved for public release: distribution unlimited.

13. SUPPLEMENTARY NOTES
ORCID ID: Jonathan Ligda, 0000-0003-3539-8867

14. ABSTRACT
Two of silicon carbide's most prominent polytypes (6H and 4H) are difficult to differentiate between experimentally. The typical techniques for identifying the polytypes are X-ray diffraction and Raman spectroscopy. While both are useful for this task, they lack the spatial resolution to analyze sub-micron features in detail. Utilizing electron backscatter diffraction improves the resolution but the polytype identification can be difficult. For this work two indexing methods are compared, the traditional Hough-style indexing and a new dictionary indexing. Increasing the number of bands used in the Hough method improves the confidence index but the dictionary method shows the best results.

15. SUBJECT TERMS
Sciences of Extreme Materials, electron backscatter diffraction, silicon carbide, polytype, dictionary indexing

16. SECURITY CLASSIFICATION OF:			17. LIMITATION OF ABSTRACT	18. NUMBER OF PAGES
a. REPORT	b. ABSTRACT	C. THIS PAGE		
UNCLASSIFIED	UNCLASSIFIED	UNCLASSIFIED	UU	18

19a. NAME OF RESPONSIBLE PERSON	19b. PHONE NUMBER *(Include area code)*
Jonathan Ligda	(410) 306-4786

STANDARD FORM 298 (REV. 5/2020)
Prescribed by ANSI Std. Z39.18

Contents

List of Figures

1. Introduction

Silicon carbide (SiC) is a well-known ceramic, notable for its low density but high hardness and fracture toughness.[1–3] One of the other features of SiC is the number of polytypes that have been found in nature—upward of 250.[4] However, some polytypes are more common than others. The two most common are the 6H and 4H polytype, here the H represents their hexagonal crystal structure. Other, less common polytypes are the cubic β-SiC (3C) or the rhombohedral (15R).[4] The 6H and 4H polytypes are the two most commonly found in production and while both are hexagonal their structure differs in their stacking order.

All hexagonal SiC is made up of alternating layers of silicon and carbon and it is their stacking order that creates the different polytypes.[5] For example, the stacking pattern in the 6H polytype is ABCACB while for 4H it is ABCB. This results in a larger unit cell for the 6H polytype specifically along the c-axis. The similarity between these two hexagonal polytypes makes it difficult to differentiate experimentally. X-ray diffraction (XRD) is the most frequently used technique for identifying SiC polytypes.[6] Another, useful technique for polytype identification is Raman spectroscopy, which detects specific vibrational modes in lattice structure.[7,8] The vibrational modes excited by Raman spectroscopy depend on the structure. SiC polytypes show excitation peaks in the 200–1000 cm^{-1} range that correspond to folding transverse acoustic/folding transverse optical (FTA/FTO) modes and folding longitudinal acoustic/folding longitudinal optical (FLA/FLO) modes.[8] For example, the 4H and 6H polytypes both have peaks near 800 cm^{-1} and can be used to differentiate between the polytypes. These methods are effective at distinguishing between SiC polytypes, but they lack the spatial resolution to determine it at the grain level.

One technique that can determine the polytype with high spatial resolution is electron backscatter diffraction (EBSD) since it uses an electron microscope.[9,10] The process for EBSD involves directing a focused electron beam onto a sample surface. The scattered electrons inside the crystal are diffracted along crystallographic planes and eventually exit the surface. That diffraction pattern, which is related to the crystal structure, is captured by a camera and an analysis software indexes it as a specific crystal orientation. Traditionally, the method for indexing an electron backscatter diffraction pattern (EBSP) first starts with performing a Hough transform on the image. This process transforms the image of the diffraction bands into bright spots that are easier for a computer to find. Once the spots are located, the next step is to compare the location and angles of the experimental spots to expected values for a given material phase.

The closest expected values are then chosen as the spot's crystallographic orientation. This indexing procedure continues point-by-point building up an entire map. This indexing procedure is effective at determining crystal orientations and is the main method used for most commercial EBSD systems. However, the disadvantage of this method arises when there are two different phases with very similar crystal structures. For example, this indexing method cannot differentiate copper (Cu) from nickel (Ni), whose lattice parameters are only roughly 0.1 Å apart.[11] To overcome this, commercial systems have incorporated chemical identification methods such as energy dispersive spectroscopy (EDS) to run concurrently with EBSD.[12]

This addition is helpful for the previous example with Cu and Ni but will not be as helpful when the two phases have a similar composition, such as with SiC polytypes. Figure 1a–1d shows examples of simulated EBSP from the basal and prismatic planes of 6H and 4H SiC polytypes. At first glance the diffraction patterns are very similar, especially when only looking at the most prominent bands. However, a closer inspection of the higher-order diffraction bands reveals minor differences between the polytypes. For the traditional indexing method to pick up such minor differences the Hough transform would need to detect many bands, which may not be possible depending on the quality of the experimental EBSP.

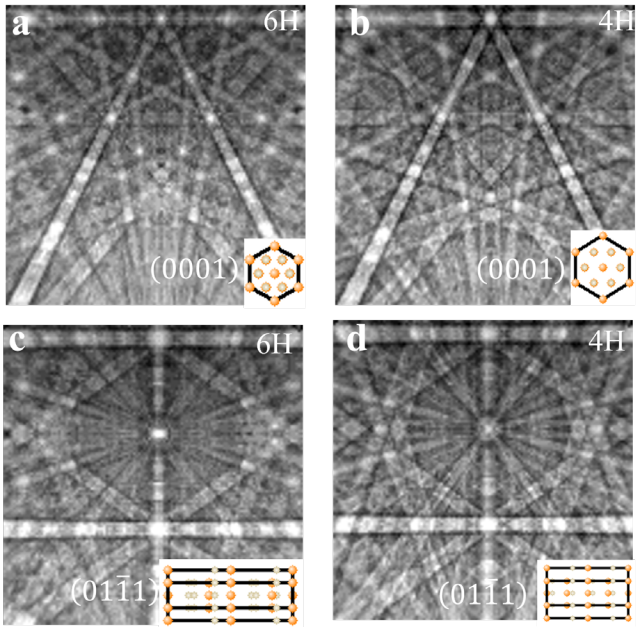

Fig. 1 Simulated EBSPs for the (a,b) basal and (c,d) prismatic planes of both 6H and 4H SiC

A new method, known as dictionary indexing, could be more accurate at differentiating between these two similar SiC polytypes.[13] Dictionary indexing is a method that has the advantage of comparing an entire experimental diffraction pattern to a dictionary list of all possible patterns for a material phase. By using the entire pattern, it could be possible to detect these minor differences in the higher-order bands and therefore differentiate between the polytypes. In this report, both the traditional and dictionary indexing methods are used to identify polytypes in SiC. The goal is to determine which method is most effective at differentiating between SiC polytypes. The results from EBSD will be compared to scans from Raman and XRD to determine if the overall polytypes are correctly identified.

2. Experiment

All data for this work is gathered from Hexoloy SiC (Saint-Gobain) that contains multiple SiC polytypes, mostly 6H and 4H. The sample is mounted in epoxy and mechanically polished to below a 1.0-µm surface finish. To determine a baseline for the type of polytypes present in this SiC sample, theta-2theta XRD scans are performed using a Bruker Discover D8 system with a Cu source (λ = 1.5406 Å). The polytypes present in the scan are analyzed using Bruker's TOPAS software. Additionally, Raman scans are done using a Horiba LabRAM Evolution equipped with a 532-nm laser and 100× objective lens. The exposure time is kept at 3 s with 10–15 total spectrum accumulations. First Raman spot scans over the 700–900 cm^{-1} range are collected on microstructural features that have a high chance of being different SiC polytypes. This range of wavenumbers is chosen because peaks for multiple polytypes are present. Second, a 16- × 25-µm Raman map with a 1.5-µm step size is done across these same features. This helps determine the location of polytypes with a higher spatial resolution than XRD affords.

However, the Raman mapping spatial resolution is still not high enough for some grain sizes, the 100× objective used for Raman only provides a 720-nm spot size, making that the step size limit for any mapping. To achieve higher resolution, EBSD is performed using a ThermoScientific Apreo Scanning Electron Microscope (SEM) equipped with an EDAX Velocity EBSD camera. The EBSD scans are done at 20 kV, 1.3 nA with a scan area of 50 × 40 µm, and a step size of 100 nm. To test the effectiveness of each indexing method the EBSP were collected at two different binning levels: 4 × 4 and 8 × 8. These correspond to image resolutions of 120 × 120 and 60 × 60 pixels, respectively. Indexing of EBSPs is done using EDAX OIM Analysis software with both the network partitioning (NPAR) and OIM Matrix add-ons. For the traditional method, trials were conducted where the number of detected bands used for re-indexing was 9 or 15, with NPAR used for both cases.

The cleanup procedure for the traditional method uses grain confidence index (CI) standardization first, followed by neighbor CI standardization. The second indexing method, dictionary indexing, is also run through OIM Analysis using the OIM Matrix add-on. A dictionary of EBSPs for both 6H and 4H SiC was created for each binning level and with a 2.5° misorientation between each simulated pattern. These dictionary lists are what the experimental patterns are compared to for indexing. To determine the effectiveness of each indexing method at determining the correct polytype the CI of each point is used.

3. Results

Figure 2 shows an SEM image of the Hexoloy SiC microstructure. There are two types of grain morphologies present in this sample: long rectangular bands that crisscross along the surface with smaller equiaxed grains in between. An XRD pattern is shown in Fig. 3, the peaks correspond to multiple SiC polytypes, including 6H, 4H, and graphite. While the XRD data provides information about the presence and amounts of the different polytypes, it does not have the spatial resolution needed to relate microstructural features to specific polytypes.

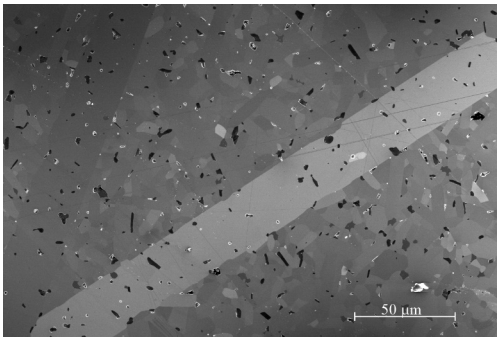

Fig. 2 SEM image showing the different grain morphologies present in this SiC sample

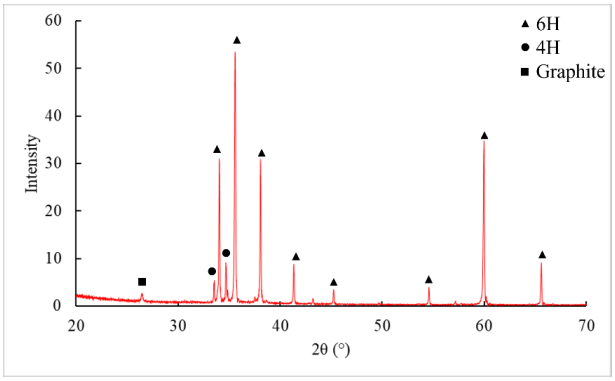

Fig. 3 XRD plot of the Hexoloy sample. Peaks from multiple SiC polytypes are present.

The Raman scans have a better spatial resolution so different microstructural features can be isolated. Figure 4a–4e shows results from Raman spot scans and a map of the Hexoloy SiC. The spectra shown in Fig. 4a are the spot scans performed in the band and equiaxed regions. While there are similarities in these two spectra, there are noticeable differences in the peak positions. The equiaxed region has peaks at 764, 784, and 794 cm^{-1}, while the band region has peaks at 779 and 794 cm^{-1}. These peaks correspond to the FTO modes of 6H and 4H SiC, respectively. This is a good indication that the different microstructure features are made up of different SiC polytypes. To determine how consistent these differences are, a Raman map was collected that spans a band and equiaxed region (Fig. 4b). The ensuing color maps indicate the height of peaks at the following positions: 794 cm^{-1} (Fig. 4c), 784 cm^{-1} (Fig. 4d), and 779 cm^{-1} (Fig. 4e).

The blue map in Fig. 4c shows the same intensity over the entire area, which is expected since this peak is present at both locations. The green map in Fig. 4d only shows intensity in the equiaxed region, while the red map (Fig. 4e) only has intensity in the band region. This confirms that the band regions in this material are 4H SiC while the equiaxed regions are 6H SiC. The Raman provides a higher spatial resolution scan compared to XRD; however, it is still lacking grain-level detail. As mentioned previously, the resolution of these scans can at best be a few hundred microns (720 nm for this specific laser and objective combination), which limits the observable feature size. Additionally, the Raman maps can take a long time to acquire. For example, the scans shown in this report took roughly 1 h with a step size of only 1.5 µm. To improve the spatial resolution, it is worth moving to using an electron beam and EBSD.

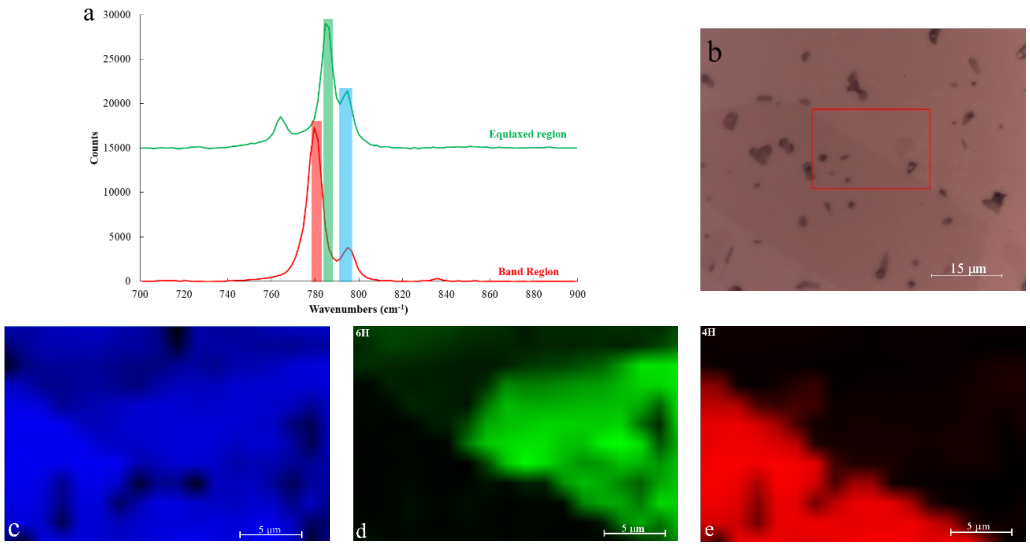

Fig. 4 (a) Raman spectra from spot scans isolated on the band and equiaxed regions. (b) Optical image showing the outline in red of the Raman map that spans a band and equiaxed region. (c–e) Color maps showing the intensity of peaks at 794 cm^{-1}, 784 cm^{-1}, and 779 cm^{-1}, respectively.

Figures 5 and 6 shows the results of a comparison between traditional Hough-based and the new dictionary-based indexing methods for EBSD. Figure 5a–5f shows the inverse pole figure (IPF) and polytype maps for the 8 × 8 binned experimental diffraction patterns. In the polytype maps the green regions are 6H SiC while the red regions are 4H SiC. Figure 5a and 5b are from the Hough indexing using 9 bands, Fig. 5c and 5d from the Hough indexing using 15 bands, and Fig. 5e and 5f are from the dictionary indexing (OIM Matrix). The first thing to note is that the map indexed using only nine bands is very noisy even after cleanup steps. The overall appearance of the microstructure is present but there is no consistency within the grains. Polytype identification is noisy for this method as well, there is no consistency for regions known to be 4H versus 6H. Increasing the number of bands used during indexing reduces the noisiness but many points are still incorrectly indexed. The polytype identification has also improved but there are still issues with correctly identifying the polytype in the band region. Finally, the dictionary indexing shows the least-noisy images out of the three with the polytype identification within each region being consistent.

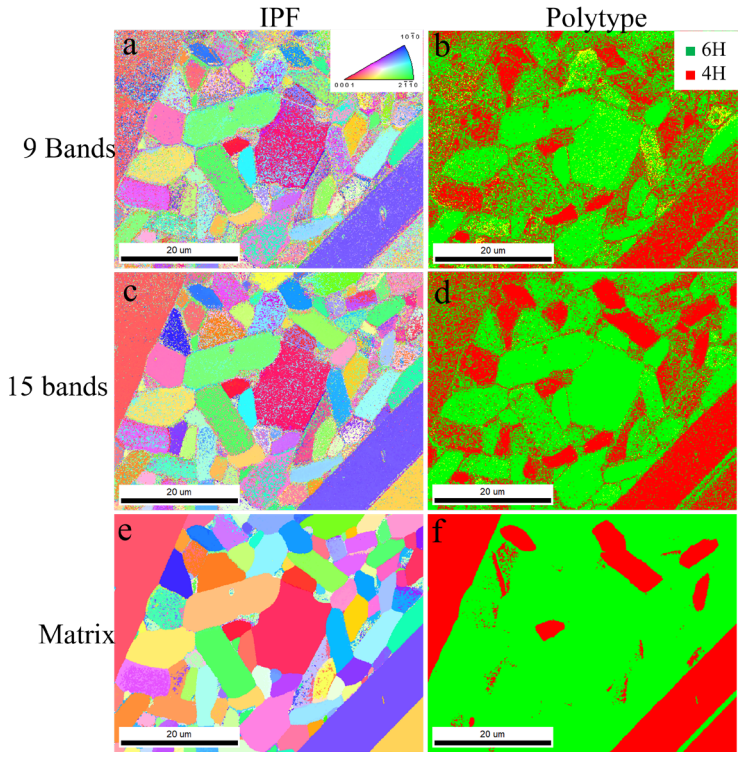

Fig. 5 (a–f) EBSD results from the 8 × 8 binned experimental patterns indexed using both the traditional and matrix methods

Figure 6a–6f shows the indexing results for diffraction patterns captured at 4 × 4 binning. The trend is similar to what was observed for the higher binned images. Hough-style indexing with only nine bands (Fig. 6a and 6b) results in the noisiest images for both orientation and polytype. When the number of bands used for indexing increases to 15 (Fig. 6c and 6d) the noise is reduced compared to the previous image but has not been removed completely. Additionally, the polytype identification in the band region is still not consistent when indexed using the Hough method. The dictionary indexing (Fig. 6e and 6f) again shows the best qualitative results for this sample. There is very little noise in the IPF maps and the polytype maps are consistent within each microstructural feature.

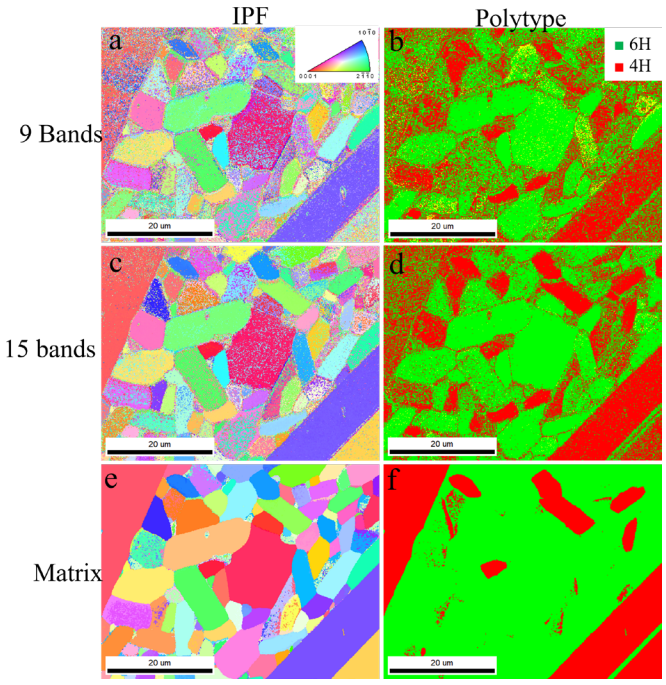

Fig. 6 (a–f) EBSD results from the 4 × 4 binned experimental patterns indexed using both the traditional and matrix methods

Figure 7a–7c shows maps of the CI for each map, a more quantitative depiction of the difference between indexing methods. For these maps, blue regions have a low confidence and red regions have high confidence. Both maps from the Hough-indexing method are mostly blue, indicating a low CI overall. The OIM Matrix indexed map in comparison is mostly red, indicating a high confidence. This is especially true for the band regions, which have a consistently high confidence index for the Matrix method but a low confidence for the traditional method.

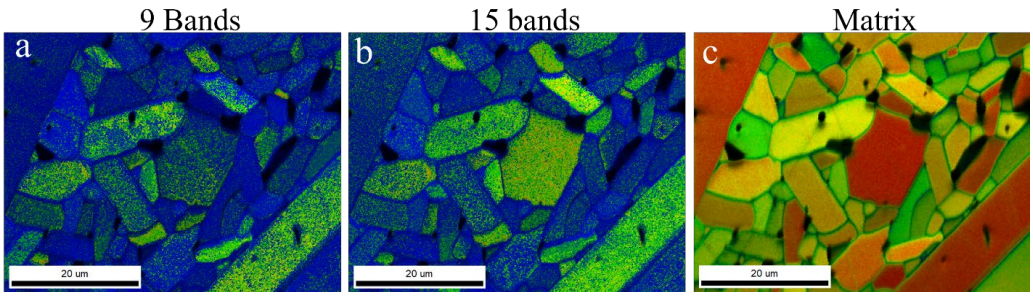

Fig. 7 (a–c) Maps showing the CI for the different indexing methods

4. Discussion

Properly identifying the polytypes of SiC with most techniques is difficult due to similarity of their crystal structure and doing so with high spatial resolution is even more difficult. Raman spectroscopy is capable of differentiating between the SiC polytypes but the spatial resolution of a typical laboratory setup is limited by the system's optics and laser. Using EBSD, individual grains and grain boundaries can be investigated but the differences in the SiC diffraction patterns are not visible unless higher-order reflections are taken into account. This means that the phase identification of traditional EBSD can be improved by increasing the number of bands used in the indexing. For example, going from using 9 to 15 bands for the traditional Hough-style indexing results in an increase in the CI. Switching to the dictionary-indexing method produces maps with the most consistent results for both orientation and polytype. Both methods are effective at indexing the diffraction patterns from SiC at both binning levels, but the matrix method gives the most confident results.

This confidence is confirmed by comparing the polytype identification between Raman and EBSD. Raman spectroscopy is already a trusted method for identification of SiC polytypes and the scans performed here confirmed that the band regions comprise 4H SiC while the equiaxed region is predominantly 6H SiC. For the traditional indexing method using 15 bands, if only looking at the IPF maps it would seem like there is a high level of confidence since there is less scattering in the band region (Fig. 6c). However, those same regions in the polytype map (Fig. 6d) shift between 4H and 6H, meaning the indexing procedure cannot consistently determine the polytype. Looking into those same regions for the dictionary indexing shows the improvement in polytype identification. For both pattern binning levels (Figs. 5e and 5f and Fig. 6e and 6f) there is consistent identification of orientation and polytype within a grain. Moreover, the polytype of the band region is 4H and the equiaxed is 6H, which agrees with the Raman results.

Another factor affecting the indexing methods is the time required to perform the calculations. Regardless of binning level, the traditional Hough-indexing procedure runs faster, which can influence what method to use. While the dictionary method is more accurate at distinguishing between polytypes, it comes with the downside of being time consuming. With the current setup (i.e., computer and software version) each dictionary re-indexing procedure can take hours to complete—making this method more situational in its usefulness. The user must decide if the improved accuracy in polytype identification is worth the additional time needed to properly index the patterns.

5. Conclusion

Differentiating between two of the most common SiC polytypes (6H and 4H) is difficult and usually requires the use of XRD or Raman spectra. Utilizing EBSD for identifying polytypes improves on the spatial resolution the two previous techniques lack. From this report, increasing the number of bands used for the traditional Hough-style indexing will improve the polytype identification. Alternatively, dictionary indexing is a new method of indexing EBD patterns that utilizes the entire pattern, not just the most prominent bands the way traditional indexing does. This aids in properly differentiating between patterns generated by these two polytypes. These results are encouraging, and the next step is to investigate if dictionary indexing can differentiate between the rarer SiC polytypes (e.g., 15R or 3C).

6. References

1. Clayton JD. Penetration resistance of armor ceramics: dimensional analysis and property correlations. Int J Impact Eng. 2015;124–131.
2. Dresch AB, Venturini J, Arcaro S, Montedo ORK, Bergmann CP. Ballistic ceramics and analysis of their mechanical properties for armour applications: a review. Ceram Int. 2021;8743–8761.
3. Holmquist TJ, Rajendran AM, Templeton DW, Bishnoi KD. A Ceramic Armor Material Database. TACOM Research Development and Engineering Center (US); 1999.
4. Bechstedt F, Käckell P, Zywietz A, Karch K, Adolph B, Tenelsen K, Furthmüller J. Polytypism and properties of silicon carbide. Physica Status Solidi B. 1997;35–62.
5. Yang B, Deng Q, Su Y, Peng X, Huang C, Lee A, Hu N. The effects of atomic arrangements on mechanical properties of 2H, 3C, 4H and 6H-SiC. Comp Mater Sci. 2022;111114.
6. Ortiz AL, Sánchez-Bajo F, Cumbrera FL, Guiberteau F. X-ray powder diffraction analysis of a silicon carbide-based ceramic. Mater Lett. 2001;137–145.
7. Nakashima S-I, Higashihira M, Maeda K, Tanaka H. Raman scattering characterization of polytype in silicon carbide ceramics: comparison with X-ray diffraction. J Am Ceram Soc. 2003;823–829.
8. Nakashima S, Harima H. Raman investigation of SiC polytypes. Physica Status Solidi A. 1997;39–64.
9. Wright SI, Adams BL. Automatic analysis of electron backscatter diffraction patterns. Metall Trans A. 1992;759–767.
10. Schwartz AJ, Kumar M, Adams BL, Field DP, editors. Electron backscatter diffraction in materials science. Springer; 2009.
11. Wright SI, Nowell MM. Improvements in the characterization of multiphase materials by automated electron backscatter diffraction [accessed 2023 Oct 5]. https://www.edax.com//media/ametekedax/files/ebsd/presentations/improvement_characterization_multiphase_materials.pdf?la=en&revision=7d8353cf-819a-4e4d-89c4-9e09437316ed.
12. Nowell MM, Wright SI. Phase differentiation via combined EBSD and XEDS. J Microsc-Oxford. 2004;296–305.
13. Chen YH, Park SU, Wei D, Newstadt G, Jackson MA, Simmons JP, De Graef M, Hero AO. A dictionary approach to electron backscatter diffraction indexing. Microsc Microanal. 2015;739–752.

List of Symbols, Abbreviations, and Acronyms

CI	confidence index
Cu	copper
EBSD	electron backscatter diffraction
EBSP	electron backscatter diffraction pattern
EDS	electron dispersion spectroscopy
FLA	folder longitudinal acoustic
FLO	folder longitudinal optical
FTA	folding transverse acoustic
FTO	folding transverse optical
IPF	inverse pole figure
Ni	nickel
NPAR	network partitioning
SEM	scanning electron microscope
SiC	silicon carbide
XRD	X-ray diffraction

1 (PDF)	DEFENSE TECHNICAL INFORMATION CTR DTIC OCA
1 (PDF)	DEVCOM ARL FCDD RLB CI TECH LIB
7 (PDF)	DEVCOM ARL FCDD RLA CB J LASALVIA FCDD RLA M K BEHLER FCDD RLA MB J LIGDA D O’BRIEN FCDD RLA ME L VARGAS-GONZALEZ T MOORE S HIRSCH